

Demography and dispersal at a grass-shrub ecotone: a spatial integral projection model for woody plant encroachment

Trevor Drees^a, Brad M. Ochocki^b, Scott L. Collins^c, and Tom E.X. Miller^{*b}

^aDepartment of Biology, Penn State University, State College, PA USA

^bProgram in Ecology and Evolutionary Biology, Department of BioSciences, Rice University, Houston, TX USA

^cDepartment of Biology, University of New Mexico, Albuquerque, NM USA

March 28, 2023

* Corresponding author: tom.miller@rice.edu

Submitted to *Ecological Monographs*

Manuscript type: Article

Open Research statement: Data are provided in Ochocki et al. (2023) and analysis code is archived in Drees and Miller (2023).

Abstract

The encroachment of woody plants into grasslands is a global phenomenon with implications for biodiversity and ecosystem function. Understanding and predicting the pace of expansion and the underlying processes that control it are key challenges in the study and management of woody encroachment. Theory from spatial population biology predicts that the occurrence and speed of population expansion should depend sensitively on the nature of conspecific density dependence. If fitness is maximized at the low-density encroachment edge then shrub expansion should be “pulled” forward. However, encroaching shrubs have been shown to exhibit positive feedbacks, whereby shrub establishment modifies the environment in ways that facilitate further shrub recruitment and survival. In this case there may be a fitness cost to shrubs at low density causing expansion to be “pushed” from behind the leading edge. We studied the spatial dynamics of creosotebush (*Larrea tridentata*), which has a history of encroachment into Chihuahuan Desert grasslands over the past century. We used demographic data from observational censuses and seedling transplant experiments to test the strength and direction of density dependence in shrub fitness along a gradient of shrub density at the grass-shrub ecotone. We also used seed-drop experiments and wind data to construct a mechanistic seed dispersal kernel, then connected demography and dispersal data within a spatial integral projection model (SIPM) to predict the dynamics of shrub expansion. The SIPM predicted that, contrary to expectations based on potential for positive feedbacks, the shrub encroachment wave is “pulled” by maximum fitness at the low-density front. However, the predicted pace of expansion was strikingly slow (ca. 8 cm/yr), and this prediction was supported by independent re-surveys of the ecotone showing little to no change in spatial extent of shrub cover over 12 years. Encroachment

25 speed was acutely sensitive to seedling recruitment, suggesting that this population may
26 be primed for pulses of expansion under conditions that are favorable for recruitment.
27 Our integration of observations, experiments, and modeling reveals not only that this
28 ecotone is effectively stalled under current conditions, but also *why* that is so and how
29 that may change as the environment changes.

30 **Keywords**

31 density-dependence, ecotones, woody encroachment, shrubs, integral projection model,
32 dispersal, Allee effects

Introduction

The recent and ongoing encroachment of shrubs and other woody plants into adjacent grasslands has caused significant vegetation changes across arid and semi-arid landscapes worldwide (Cabral et al., 2003; Gibbens et al., 2005; Goslee et al., 2003; Parizek et al., 2002; Roques et al., 2001; Trollope et al., 1989; Van Auken, 2009, 2000). The process of encroachment generally involves increases in the number or density of woody plants in both time and space (Van Auken, 2000), which can drive shifts in plant community structure and alter ecosystem processes (Knapp et al., 2008; Ravi et al., 2009; Schlesinger and Pilmanis, 1998; Schlesinger et al., 1990). Other effects of encroachment include changes in ecosystem services (Kelleway et al., 2017; Reed et al., 2015), declines in biodiversity (Brandt et al., 2013; Ratajczak et al., 2012; Sirami and Monadjem, 2012), and economic losses in areas where the proliferation of shrubs adversely affects grazing land and pastoral production (Morford et al., 2022).

Woody plant encroachment can be studied through the lens of spatial population biology as a wave of individuals that may expand across space and over time (Kot et al., 1996; Neubert and Caswell, 2000; Pan and Lin, 2012; Wang et al., 2002). Theory predicts that whether the wave can advance and the speed at which it does so depends on two processes: local demography and dispersal of propagules. First, local demographic processes include recruitment, survival, growth, and reproduction, which collectively determine the rate at which newly colonized locations increase in density and produce new propagules. Second, colonization events are driven by the spatial dispersal of propagules, which is commonly summarized as a probability distribution of dispersal distances, or “dispersal kernel”. Expansion speed is highly dependent upon the shape of the dispersal kernel and can be strongly influenced by long-distance dispersal events in the tail

57 of the distribution (Skarpaas and Shea, 2007). Both demography and dispersal may de-
58 pend on plant size, since larger plants often have improved demographic performance
59 and release seeds from greater heights, leading to longer dispersal distances (Nathan
60 et al., 2011). Accounting for population structure, including size structure, may therefore
61 be important for understanding and predicting encroachment dynamics (Neubert and
62 Caswell, 2000).

63 Theory predicts that the nature of conspecific density dependence is another crit-
64 ical feature of expansion dynamics but this is rarely studied in the context of woody
65 plant encroachment. Expansion waves typically correspond to gradients of conspecific
66 density – high in the back and low at the front – and demographic rates may be sen-
67 sitive to density due to intraspecific interactions like competition or facilitation. If the
68 demographic effects of density are strictly negative due to competitive effects that in-
69 crease with density, then demographic performance is expected to be maximized as den-
70 sity goes to zero at the leading edge of the wave. Under these conditions, the wave is
71 “pulled” forward by individuals at the low-density vanguard (Kot et al., 1996), and tar-
72 geting these individuals and locations would be the most effective way to slow down or
73 prevent encroachment. However, woody encroachment often involves positive feedbacks
74 whereby shrub establishment modifies the environment in ways that facilitate further
75 shrub recruitment. For example, woody plants can modify their micro-climates in ways
76 that elevate nighttime minimum temperatures, promoting conspecific recruitment and
77 survival for freeze-sensitive species (D’odorico et al., 2013; Huang et al., 2020). Posi-
78 tive density dependence (or Allee effects) causes demographic rates to be maximized at
79 higher densities behind the leading edge, which “push” the expansion forward, leading
80 to qualitatively different expansion dynamics (Kot et al., 1996; Lewis and Kareiva, 1993;
81 Sullivan et al., 2017; Taylor and Hastings, 2005; Veit and Lewis, 1996). Pushed expan-

82 sion waves generally have different shapes (steeper density gradients) and slower speeds
83 than pulled waves (Gandhi et al., 2016), and may require different strategies for man-
84 aging or decelerating expansion (Taylor and Hastings, 2005). Under some conditions,
85 pushed waves may fail entirely, “pinning” population boundaries in place (Keitt et al.,
86 2001). The potential for positive feedbacks is well documented in woody encroachment
87 systems as a key feature of bi-stability (the existence of woody and herbaceous habitats
88 as alternative stable states: Wilcox et al. (2018)) but it remains unclear whether and how
89 strongly these feedbacks decelerate shrub expansion or prevent it altogether.

90 In this study, we linked shrub dynamics at grass-shrub ecotones to ecological theory
91 for spreading populations, with the goals of understanding the spatial dynamics that
92 emerge from seed dispersal and density-dependent demography at the edge of the en-
93 croachment wave, and determining whether the wave is pushed or pulled. Throughout
94 the aridlands of the southwestern United States, shrub encroachment into grasslands is
95 well documented (D’Odorico et al., 2012) but little is known about the dispersal and de-
96 mographic processes that govern it. Our work focused on creosotebush (*Larrea tridentata*)
97 in the northern Chihuahuan Desert. This native shrub has encroached into grasslands
98 over the past 150 years, leading to decreased cover of black grama grass (*Bouteloua eri-*
99 *opoda*), the dominant foundation species of Chihuahuan desert grassland (Buffington
100 and Herbel, 1965; Gardner, 1951; Gibbens et al., 2005). As in many woody encroachment
101 systems, creosotebush expansion generates ecotones marking a transition from dense
102 shrubland to open grassland, with a transition zone in between where shrubs can often
103 be found interspersed among grasses (Fig. 1).

104 Historically, creosotebush encroachment into grasslands is believed to have been
105 driven by a combination of factors including overgrazing, drought, variability in rain-
106 fall, and suppression of fire regimes (Moreno-de las Heras et al., 2016). These shrubs

are also thought to further facilitate their own encroachment through positive feedbacks (D’Odorico et al., 2012; Grover and Musick, 1990) by modifying their environment in ways that favor survival, growth, and recruitment, including changes to the local microclimate (D’Odorico et al., 2010) and rates of soil erosion (Turnbull et al., 2010). Such positive feedbacks also involve suppression of herbaceous competitors, reducing competition as well as the amount of flammable biomass used to fuel the fires that keep creosotebush growth in check (Van Auken, 2000).

Our work was conducted at the Sevilleta Long-Term Ecological Research (LTER) site in central New Mexico, where the most recent major advance of creosotebush into desert grassland is estimated to have occurred in the 1950s (Moreno-de las Heras et al., 2016). More recently, the shrub encroachment wave has exhibited little apparent advance. For example, between 2001 and 2013, we saw very little change in the spatial extent of shrub cover measured along two permanent transects (Fig. 2), small enough to be conservatively attributable to measurement error. We therefore sought to mechanistically understand whether this shrub encroachment wave is indeed stalled under current conditions, why that is so, and whether it is poised to remain that way. One hypothesis is that the positive feedbacks that favor bi-stability – maintaining shrubland as shrubland and grassland as grassland – may inhibit advance of the encroachment wave. This hypothesis predicts fitness penalties for shrubs at the low-density vanguard (pushed-wave dynamics). Alternatively, positive feedbacks may be absent or insufficient to prevent shrub encroachment of grassland, but the pace of encroachment may be limited by other factors. This hypothesis predicts that the encroachment wave is pulled forward (fitness maximized at low density) but may be pulled very slowly or episodically due to constraints associated with short seed dispersal and low seedling recruitment (Boyd and Brum, 1983; Moreno-de las Heras et al., 2016). Our study was designed to differentiate

132 between these competing hypotheses.

133 We used a combination of observational and experimental data from grass-shrub eco-
134 tones in central New Mexico to parameterize a spatial integral projection model (SIPM)
135 that predicts the speed of encroachment (m/yr) resulting from lower-level demographic
136 and dispersal processes. Our data came from demographic surveys and experimen-
137 tal transplants along replicate ecotone transects spanning a gradient of shrub density,
138 and from seed drop experiments to estimate the properties of the dispersal kernel. We
139 focused on wind dispersal of seeds, since little is known about the natural history of
140 dispersal in this system and the seeds lack adaptations to attract frugivorous animals,
141 such as bright coloration or fleshy fruit, though they may be moved by granivores. We
142 built mechanistic dispersal kernels that predict seed movement based on properties of
143 maternal plants, seeds, and wind; because it does not account for secondary disper-
144 sal vectors, this approach provided a conservative first step toward understanding seed
145 movement. The SIPM accounts for size-structured demography of creosotebush, allows
146 us to test whether shrub expansion is pulled by the low-density front or pushed from
147 the high-density core, and identifies the local (demographic) and spatial (seed dispersal)
148 life cycle transitions that most strongly limit encroachment. We address the following
149 specific questions:

- 150 1. What are the strength and direction of density dependence in demographic vital
151 rates along shrub encroachment ecotones?
- 152 2. What is the seed dispersal kernel and how does it vary with maternal plant size?
- 153 3. What is the predicted rate of expansion and which lower-level processes most
154 strongly affect the expansion speed?

Materials and methods

Study species

Creosotebush (*Larrea tridentata*) is a perennial, drought-resistant shrub that is native to the arid and semiarid regions of the southwestern United States and northern Mexico. High-density areas of creosotebush consist largely of barren soil between plants due to the “islands of fertility” these shrubs create around themselves (Reynolds et al., 1999; Schlesinger et al., 1996), though lower-density areas will often contain grasses in the inter-shrub spaces (Fig. 1). Elsewhere in North America creosotebush can produce clonal rings through asexual reproduction (Vasek, 1980) but this does not occur in our northern Chihuahuan desert study region, where creosotebush genetic diversity is high (Duran et al., 2005). The small yellow flowers of creosotebush give rise to pubescent spherical fruits several *mm* in diameter; these fruits consist of five carpels, each of which contains a single seed. Seeds are dispersed from the parent plant by gravity and wind, with the possibility for seeds to subsequently be transported by animals or water (Maddox and Carlquist, 1985). The foliage is dark green, resinous, and unpalatable to most grazing and browsing animals (Mabry et al., 1978).

Study site

We conducted our work at the Sevilleta National Wildlife Refuge (SNWR), a Long-Term Ecological Research (SEV-LTER) site in central New Mexico. The refuge exists at the intersection of several eco-regions, including the northern Chihuahuan Desert, Great Plains grassland, and steppes of the Colorado Plateau. Annual precipitation is approximately 250*mm*, with the majority falling during the summer monsoon from June to September.

177 The recruitment events that facilitate creosotebush expansion are thought to be episodic
178 (Peters and Yao, 2012), and this may be linked to fluctuations in monsoon precipitation
179 (Bowers et al., 2004; Boyd and Brum, 1983). SNWR has been closed to cattle grazing since
180 1973. Wildfires at SNWR are allowed to burn but there have been no major fires near the
181 grass-shrub ecotone since 2003. Our study years included one unusually wet and one
182 unusually dry monsoon season (Appendix S2: Fig. S1A).

183 *Demographic data*

184 *Ecotone transects*

185 We collected demographic data during early June of every year from 2013-2017. This
186 work was conducted at four sites in the eastern part of SNWR (one site was initiated in
187 2013 and the other three in 2014), with three transects at each site. All transects were
188 situated along a shrubland-grassland ecotone so that a full range of shrub densities was
189 captured: each transect spanned core shrub areas, grassland with no or few shrubs,
190 and the transition between them. Lengths of these transects varied from 200 to 600 m
191 and were determined by the strength of vegetation transition since “steep” transitions
192 required less length to capture the full range of shrub density.

193 We quantified shrub density in 5-meter “windows” along each transect, including all
194 shrubs within one meter of the transect on either side (shrubs that partially overlapped
195 with the census area were included). Densities were quantified once for each transect
196 (in 2013 or 2014) and were assumed to remain constant for the duration of the study, a
197 reasonable assumption for a species with very low recruitment and very high survival of
198 established plants (see Results). Given the population’s size structure, we weighted the
199 density of each window by the sizes of the plants, which we quantified as volume (cm³).
200 Volume was calculated as that of an elliptic cone (McAuliffe et al., 2007): $V_i = \frac{\pi h}{3} \frac{lw}{4}$

201 where l , w , and h are the maximum length, maximum width, and height, respectively.
202 Maximum length and width were measured so that they were always perpendicular to
203 each other, and height was measured from the base of the woody stem at the soil surface
204 to the tallest part of the shrub. The weighted density for a window was then expressed
205 as $\log(\text{volume})$ summed over all plants in the window.

206 *Observational census*

207 At approximately 50-m intervals along each transect we tagged up to 10 plants for annual
208 demographic census and recorded their local (5-m resolution) window so that we could
209 connect individual demographic performance to local density. These tagged shrubs were
210 revisited every June and censused for survival (alive/dead), size (width, length, and
211 height, as above), flowering status, and fertility of flowering plants (numbers of flower-
212 buds, flowers, and fruits). In instances where shrubs had large numbers of reproductive
213 structures that would be difficult to reliably count (a large shrub may have thousands of
214 flowers or fruits), we made counts on a fraction of the shrub and extrapolated to esti-
215 mate whole-plant reproduction. Creosotebush does not have one discrete reproductive
216 event per year; instead, flowering may occur throughout much of the warm season. By
217 combining counts of buds, flowers, and fruits we intended to capture a majority of the
218 season's reproductive output, assuming that all buds and flowers will eventually become
219 fruits. Our measurements of reproductive output are therefore conservative and may un-
220 derestimate total seed production for an entire transition year. Each year, we searched
221 for new recruits within 1m on either side of the transect. New recruits were tagged
222 and added to the demographic census. The observational census included a total of 522
223 unique individuals.

224 *Transplant experiment*

225 We conducted a transplant experiment in 2015 to test how shrub density affects seedling
226 survival. This approach complemented observational estimates of density dependence
227 and filled in gaps for a part of the shrub life cycle that was rarely observed due to low
228 recruitment. Seeds for the experiment were collected from plants in our study popu-
229 lation in 2014. Seeds were germinated on Pro-Mix potting soil (Quakertown, PA) in
230 Fall 2014 and seedlings were transferred to 3.8 cm-by-12.7 cm cylindrical containers and
231 maintained in a greenhouse at Rice University. Seedlings were transported to SNWR
232 and transplanted into the experiment during July 27-31, 2015. Transplant timing was
233 intended to coincide with the monsoon season, when most natural recruitment occurs.

234 The transplant experiment was conducted at the same four sites and three transects
235 per site as the observational demographic census, where we knew weighted shrub den-
236 sities at 5-m window resolution. We established 12 1-m by 1-m plots along each transect
237 and these were intentionally placed to capture density variation: four plots were in win-
238 dows with zero shrubs, four plots were placed in the top four highest-density windows
239 on the transect, and the remaining four plots were randomly distributed among the re-
240 maining windows with weighted density greater than zero. Plots were placed in the
241 middle of each 5-m window (at meter 2.5) and were divided into four 0.5-m by 0.5-m
242 subplots. We divided each subplot into nine squares (0.125-m by 0.125-m) and recorded
243 ground cover of each square as one of the following categories: bare ground, creosote-
244 bush, black grama (*B. eriopoda*), blue grama (*B. gracilis*), other grass, or “other”. Each
245 subplot received one transplanted shrub seedling, for a total of 48 transplants per tran-
246 sect, 144 transplants per site, and 576 transplants in the entire experiment. Each site was
247 set up on a different day and there was a significant monsoon event between setup of the
248 third and fourth sites. This resulted in differential mortality that appears to be related

249 to site (captured as a statistical random effect) but more likely reflects the timing of the
250 monsoon event relative to planting (moist soil likely promoted transplant survival). We
251 revisited the transplant experiment on October 24, 2015 to survey mortality. After that
252 first visit, transplants were censused along with the naturally occurring plants each June,
253 following the methods described above.

254 *Demographic analysis*

255 We fit statistical models to the demographic data and used AIC-based model selection to
256 evaluate empirical support for alternative candidate models. The top statistical models
257 were then used as the vital rate sub-models of the SIPM, so there is a strong connection
258 between the statistical and population modeling, as is typical of integral projection mod-
259 eling. Our analyses focused on the following demographic vital rates: survival, growth,
260 probability of flowering, fertility (flower and fruit production), seedling recruitment, and
261 seedling size. Most of these vital rates were modeled as a function of plant size, and all
262 of them included the possibility of density dependence.

263 The alternative hypotheses of pushed versus pulled wave expansion rest on how the
264 rate of population increase (λ), derived from the combination of all vital rates, respond
265 to density. We were particularly interested in whether demographic performance was
266 maximized as local density goes to zero (pulled) or at non-zero densities behind the
267 wave front (pushed). To flexibly model density dependence and detect non-monotonic
268 responses, we used generalized additive models in the R package ‘mgcv’ (Wood, 2017).
269 For each vital rate, we fit candidate models with or without a smooth term for local
270 weighted density, among other possible covariates. To avoid over-fitting, we set the
271 ‘gamma’ argument of gam() to 1.8, which increases the complexity penalty, results in
272 smoother fits (Wood, 2017), and makes our approach more conservative (other gamma

values yielded qualitatively similar results). We pooled data across transition years for analysis. All models included the random effect of transect (12 transects across 4 sites); we did not attempt to model both site and transect-within-site random effects due to the low numbers of each. All vital rate functions used the natural logarithm of volume (cm^3) as the size variable and the sum of $\log(\text{volume})$ as the weighted density of a transect window.

Survival. We modeled survival (alive or dead) in year $t + 1$ as a Bernoulli random variable with three candidate models for survival probability. These included smooth terms for initial size in year t only (1), initial size and weighted density (2), and both smooth terms plus an interaction between initial size and weighted density (3). We analyzed survival of experimental transplants and observational census plants together in the same analyses, with a fixed effect of transplant status (yes/no) included in all candidate models. Since recruits and thus mortality events were both very rare in the observational survey, this approach allowed us to “borrow strength” over both data sets to generate a predictive function for size- and possibly density-dependent survival while statistically accounting for differences between experimental and naturally occurring plants. Because we had additional, finer-grained cover data for the transplant experiment that we did not have for the observational census, we conducted an additional stand-alone analysis of transplant survival that explored the influence of shrub and grass density at multiple spatial scales (Appendix S3).

Growth. We modeled size in year $t + 1$ (a continuous variable) as a Gaussian random variable, with nine candidate models for growth. The simplest model (1) defined the mean of size in year $t + 1$ as a smooth function of size in year t and constant variance. Models (2) and (3) had constant variance but the mean included smooth terms for initial

size and weighted density (2) or both smooth terms plus an interaction between initial size and weighted density (3). Models 4-6 had the same mean structure as 1-3 but defined the standard deviation of size in year $t + 1$ as a smooth function of initial size. Models 7-9 mirrored 4-6 and additionally included a smooth term for weighted density in the standard deviation. Modeling growth correctly is important because it defines the probability of any future size conditional on current size, a critical element of the IPM transition kernel. We verified that the AIC-selected model described the data well by simulating data from it and comparing the moments (mean, variance, skewness, and kurtosis) of simulated and real data.

Flowering and fruit production. We modeled shrub reproductive status (vegetative or flowering) in year t as a Bernoulli random variable with three candidate models for flowering probability. These included smooth terms for current size (in year t) only (1), size and weighted density (3), and both smooth terms plus an interaction between size and weighted density. We modeled the reproductive output of flowering plants (the sum of flowerbuds, open flowers, and fruits) in year t as a negative binomial random variable. There were three candidate models for mean reproductive output that corresponded to the same three candidates for flowering probability.

Recruitment and recruit size. We modeled seedling recruitment in each transect window as a binomial random variable given the number of seeds (successes) and the total seeds produced in that window in the preceding year (trials). There were two candidate models, with and without an influence of weighted density on the per-seed recruitment probability. To estimate window-level seed production, we used the best-fit models for flowering and fruit production and applied this to all plants in each window that we observed in our initial density surveys. We assume that recruits come from the previous

year's seeds and not from a long-lived soil seed bank. This assumption might lead us to over-estimate the recruitment rate, since existence of a seed bank would inflate the denominator of seedlings-per-seed. However, a previous study at SNWR found relatively low densities of viable creosotebush seeds in soil, suggesting that this species does not form a persistent seed bank (Moreno-de las Heras et al., 2016). Our estimation of recruitment combines the processes of seed germination and early seedling survival preceding the census.

We modeled recruit size (a continuous variable) as a Gaussian-distributed random variable and fit four candidate models including an influence of weighted density on mean, variance, both, and neither.

Density-dependent IPM

The size- and density-dependent statistical models comprised the sub-models of a density dependent Integral Projection Model (IPM) that we used to evaluate how the shrub population growth rate responded to conspecific density; we present this non-spatial model before layering on the spatial dynamics generated by seed dispersal. A basic density-independent IPM predicts the number of individuals of size x' at time $t + 1$ ($n(x', t + 1)$) based on a demographic projection kernel (K_{dem}) that gives the rates of transition from sizes x to x' from times t to $t + 1$ and is integrated over the size distribution from the minimum (x_{min}) to maximum (x_{max}) sizes. In a density-dependent IPM, components of the projection kernel may respond to population abundance and structure:

$$n(x', t + 1) = \int_{x_{min}}^{x_{max}} K_{dem}(x', x, \tilde{n}(t)) n(x, t) dx \quad (1)$$

Here, $\tilde{n}(t)$ is some function of population structure $n(x, t)$ such as the total density of conspecifics ($\tilde{n}(t) = \int n(x, t) dx$) or, as in our case, total density weighted by size ($\tilde{n}(t) =$

344 $\int x n(x, t) dx$). For simplicity, in the analyses that follow we do not model density as
 345 a dynamic state variable; instead, we treat density as a static covariate ($\tilde{n}(t) = \tilde{n}$) and
 346 evaluate the IPM at a range of density values. As in our statistical modeling, the size
 347 variable of the IPM (x, x') was $\log(\text{cm}^3)$.

348 For our model, the size- and density-dependent demographic transitions captured by
 349 the projection kernel include growth or shrinkage (g) from size x to x' conditioned on
 350 survival (s) at size x (combined growth-survival function $G(x', x, \tilde{n}) = g(x', x, \tilde{n})s(x, \tilde{n})$),
 351 and the production of new size- x' individuals from size- x parents ($Q(x', x, \tilde{n})$). Repro-
 352 duction reflects the probability of flowering at size x (p), the number of seeds produced
 353 by flowering plants (d), the per-seed probability of recruitment (m), and the size distri-
 354 bution of recruits (c). Collectively, the rate at which x -sized individuals produce x' -sized
 355 individuals at density \tilde{n} is given by the combined reproduction-recruitment function
 356 $Q(x', x, \tilde{n}) = p(x, \tilde{n})d(x, \tilde{n})m(\tilde{n})c(x', \tilde{n})$. Thus, we can express the projection kernel as:

$$357 \quad K_{dem}(x', x, \tilde{n}) = G(x', x, \tilde{n}) + Q(x', x, \tilde{n}) \quad (2)$$

358 For analysis, we evaluated the IPM kernel over a range of local densities from the min-
 359 imum to the maximum of weighted density values observed in the 5-meter windows
 360 ($0 \leq \tilde{n} \leq \tilde{n}_{max}$). At each density level, we discretized the IPM kernel into a 200×200
 361 matrix and calculated the asymptotic growth rate $\lambda(\tilde{n})$ as its leading eigenvalue. We ex-
 362 tended the lower (x_{min}) and upper (x_{max}) integration limits to avoid unintentional “evic-
 363 tion” using the floor-and-ceiling method (Williams et al., 2012).

364 We sought to characterize the shape of density dependence – whether fitness de-
 365 clined monotonically or not with increasing density – and quantified uncertainty in the
 366 density-dependent growth rate $\lambda(\tilde{n})$ by bootstrapping our data. For each bootstrap, we
 367 randomly sampled 75% of our demographic data, re-ran the statistical modeling and

368 model selection, and used the top vital rate models to generate $\lambda(\tilde{n})$ for that data subset.
 369 We repeated this procedure for 500 bootstrap replicates.

370 *Dispersal modelling*

371 *WALD dispersal model.* Dispersal kernels were calculated using the WALD, or Wald ana-
 372 lytical long-distance dispersal, model that uses a mechanistic approach to predict disper-
 373 sal patterns of plant propagules by wind. The WALD model, which is based in fluid dy-
 374 namics, can serve as a good approximation of empirically-determined dispersal kernels
 375 (Katul et al., 2005; Skarpaas and Shea, 2007) and may be used when direct observations
 376 of dispersal are not available. Under the assumptions that wind turbulence is low, wind
 377 flow is vertically homogenous, and terminal velocity is achieved immediately upon seed
 378 release, the WALD model simplifies a Lagrangian stochastic model to create a dispersal
 379 kernel that estimates the likelihood a propagule will travel a given distance (Katul et al.,
 380 2005). Our dispersal kernel takes the form of the inverse Gaussian distribution, using r
 381 to denote dispersal distance:

$$382 \quad p(r) = \left(\frac{\lambda'}{2\pi r^3} \right)^{\frac{1}{2}} \exp \left[-\frac{\lambda'(r - \mu')^2}{2\mu'^2 r} \right] \quad (3)$$

383 Here, λ' is the location parameter and μ' is the scale parameter, which depend on
 384 environmental and plant-specific properties of the study system. (We use λ' for consis-
 385 tency with notation in related papers, but λ' the dispersal location parameter should not
 386 be confused with λ the geometric growth rate.) The location and scale parameters are
 387 defined as $\lambda' = (H/\sigma)^2$ and $\mu' = HU/F$; these are functions of the height H of seed
 388 release, wind speed U at seed release height, seed terminal velocity F , and the turbulent
 389 flow parameter σ that depends on both wind speed and local vegetation roughness. We
 390 parameterized the WALD dispersal kernel using windspeed data from the SEV-LTER

weather station nearest our study site (Moore and Hall, 2022) and seed terminal velocity data from laboratory-based seed-drop experiments (Appendix S1). We integrated the dispersal kernel over observed variation in wind speeds, seed terminal velocity, and release height within the height of a shrub. Therefore the dispersal kernel for a shrub of height H was given by:

$$K_{disp} = \iiint p(F)p(U)p(z)p(r) dF dU dz \quad (4)$$

and $p(F)$ and $p(U)$ are the PDFs of the terminal velocity F and wind speed U , respectively, and $p(z)$ is the uniform distribution from the minimum seed release height ($0.15m$, the height at which grass cover interferes with wind dispersal) to H . Methods for our seed data collection and technical details of dispersal kernel modeling are provided in Appendix S1.

Spatial integral projection model

We used a spatial integral projection model to piece together seed dispersal and density-dependent demography, and generate predictions for the rate of shrub expansion that results from this combination of local and spatial processes. The spatially explicit model builds upon the non-spatial model (Eq. 1) and adds a spatial variable (z, z') such that demographic transitions occur across both time and space according to a combined demography-dispersal kernel \tilde{K} :

$$n(x', z', t + 1) = \int_{-\infty}^{+\infty} \int_{x_{min}}^{x_{max}} \tilde{K}(x', x, z', z, \tilde{n}(z, t)) n(x, z, t) dx dz \quad (5)$$

Here, $\tilde{K}(x', x, z', z, \tilde{n}(z, t))$ describes the transition from size x and location z to size x' and location z' given density $\tilde{n}(z, t)$ at starting location z . As before, \tilde{n} is a function of

412 population structure – in our model, weighted local density – but here integrated over
 413 an explicit competitive “neighborhood”:

$$414 \quad \tilde{n}(z, t) = \int_{z-h}^{z+h} \int_{x_{min}}^{x_{max}} x n(x, z, t) dx dz \quad (6)$$

415 where h represents neighborhood size in the units of z . The demography-dispersal
 416 kernel \tilde{K} is given by the sum of two parts, one that describes reproduction coupled
 417 with dispersal of propagules, and another that describes growth and survival of non-
 418 dispersing individuals:

$$419 \quad \tilde{K}(x', x, z', z, \tilde{n}(z, t)) = K_{disp}(z' - z)Q(x', x, \tilde{n}) + \delta(z' - z)G(x', x, \tilde{n}) \quad (7)$$

420 Here, the regeneration function Q and growth-survival function G correspond to Eq.
 421 2, dispersal kernel K_{disp} corresponds to Eq. 7, and the Dirac delta function ($\delta(z' - z)$) is a
 422 probability distribution with all mass at zero, which prevents movement during survival
 423 and size transition. Following standard assumptions for integro-difference equations,
 424 we assume that space is one-dimensional and homogeneous, such that demographic
 425 transitions do not depend on location (or, more precisely, that they depend on location
 426 only through spatial variation in density) and the probability of dispersing from location
 427 z to z' depends only on the absolute distance between them.

428 Under many conditions, models of this form generate traveling waves, and we are
 429 particularly interested in the velocity (m/yr) of this wave. Methods to estimate this ve-
 430 locity depend strongly on how demography responds to density. If fitness is maximized
 431 at some density $\tilde{n} > 0$ then the wave is pushed and wave velocity can only be estimated
 432 through numerical simulation. However, if fitness is maximized at $\tilde{n} = 0$ then the wave
 433 is pulled and an upper bound on its asymptotic velocity can be calculated analytically,

434 following Neubert and Caswell (2000) and Jongejans et al. (2011), as

$$435 \quad c^* = \min_{s>0} \left[\frac{1}{s} \ln(\rho_s) \right] \quad (8)$$

436 where s is a wave shape parameter and ρ_s is the dominant eigenvalue of the kernel
 437 $H_s(x', x)$. Corresponding to Eq. 7 and assuming $\tilde{n} = 0$, H_s is composed of

$$438 \quad H_s(x', x) = M(s, x)Q(x', x) + G(x', x) \quad (9)$$

439 where $M(s, x)$ is the moment-generating function (MGF) for the dispersal kernel as-
 440 sociated with size x . This formulation of the model assumes that the dispersal kernel
 441 depends only on maternal size x and not offspring size x' . To estimate $M(s, x)$ we sim-
 442 ulated $N = 10000$ dispersal events (r) for each size x and marginalized these over one
 443 spatial dimension as in Lewis et al. (2006). We then evaluated the empirical MGF for
 444 each size x : $M(s) = \frac{1}{N} \sum_{i=1}^N e^{sr}$.

445 We used numerical sensitivity analysis to compare the contributions of demography
 446 and dispersal processes to the speed of expansion. We perturbed each vital rate function
 447 by an arbitrary value, recalculated wavespeed, and quantified sensitivity as the change
 448 in wavespeed divided by the perturbation. Analytical sensitivity analysis is also possible
 449 (Ellner et al., 2016) but these sensitivities reflect infinitesimally small perturbations. We
 450 were particularly interested in the effects of large perturbations, especially large changes
 451 in seedling recruitment, which is subject to pulse events.

452 Estimates of wavespeed and its sensitivity to demography and dispersal processes
 453 were bootstrapped for a total of 1000 replicates. Each bootstrap replicate recreated size-
 454 and density-dependent demographic models using 50% resampling on the original de-
 455 mographic data, and recreated dispersal kernels also using 75% resampling on the wind

456 speeds and seed terminal velocities. Model selection for demographic vital rates was re-
457 run for each bootstrap replicate. The empirical MGF relied on numerical sampling and
458 was therefore sensitive to extreme long-distance events that differed across bootstrap
459 realizations. Therefore, bootstrapped distributions reflect the combination of model un-
460 certainty, parameter uncertainty, and stochasticity inherent to empirical MGFs.

461 Results

462 *What are the strength and direction of density dependence in*
463 *demographic vital rates along shrub encroachment ecotones?*

464 Demographic data from naturally occurring and transplanted individuals revealed strong
465 size- and density-dependence in demographic vital rates. For most sizes and vital rates,
466 shrub density had negative demographic effects; there was no strong evidence for posi-
467 tive density dependence in any demographic process at any size. Statistical support for
468 size- and density-dependence is provided in Appendix S2: Tables S1–S6, which provide
469 AIC rankings for candidate models based on the complete data set. In Figure 3, size is
470 discretized into four groups evenly spaced from minimum to maximum size; this is for
471 visualization purposes only.

472 *Survival.* Among naturally occurring plants, survival of large, established individuals
473 was very high (Fig. 3A). We observed relatively few mortality events and nearly all of
474 these were among new recruits. The probability of survival at these small sizes declined
475 with increasing density. Survival of transplants was very low, lower even than survival
476 of similarly-sized, naturally occurring recruits (Fig. 3A). However, the transplant results
477 support the general pattern of negative density dependence in survival. Among the

478 20 survivors, 15 of them occurred in transect windows below the median of weighted
479 shrub density. In Appendix S2, we show that transplant mortality was dominated by
480 negative effects of shrub density at the 5-m window scale, even when effects of local
481 grass and shrub cover were included as alternative or additional statistical covariates,
482 which suggests that this is the appropriate spatial scale for modeling density dependence
483 in this system.

484 *Growth.* Current size was strongly predictive of future size, as expected, and there was
485 weak negative density dependence in mean future size conditioned on current size (Fig.
486 3B). However, there was a stronger signal of density dependence in the variance of future
487 size (Fig. 3B, inset). Plants at low density exhibited greater variance in growth trajectories
488 and this was especially true at the smallest sizes. Thus, large increases (and decreases)
489 in the size of new recruits were most likely to occur under low-density conditions.

490 *Flowering and fruit production.* Flowering probability was strongly size-dependent and
491 and very weakly sensitive to local density (Fig. 3C). However, fertility of flowering plants
492 was strongly negative density dependent, with greatest flower and fruit production by
493 the largest plants at the lowest densities, and vice versa (Fig. 3D).

494 *Recruitment and recruit size.* We observed 32 natural recruitment events along our tran-
495 sects during the study years and our estimated recruitment rate, given total expected
496 seed production in each window preceding the recruitment year, was very low ($2.47 \times$
497 10^{-6} , 3E). While most recruitment events occurred at low density, this is also where
498 most seed production was concentrated (Fig. 3E), and low-density windows were over-
499 represented relative to high density. For these reasons we were more likely to observe re-
500 cruiment events at low density. Controlling for sampling effort and seed production, the

501 statistical models indicated that our data were most consistent with a constant, density-
502 independent seed-to-seedling recruitment rate (Table S6). However, the mean size of new
503 recruits declined significantly with local density (Fig. 3F).

504 *Population growth rate.* As expected given the vital rate results, the asymptotic popula-
505 tion growth rate λ declined monotonically with density (Fig. 4). This was true across
506 > 98% of bootstrap replicates, indicating high certainty that shrub fitness is maximized at
507 zero density and thus that the expansion wave is “pulled” (for this reason our wavespeed
508 results are based on the analytical approach described above). Mean growth rate at low
509 density was *ca.* 3% per year, with bootstrap uncertainty spanning 1–6%. At high density
510 in the core of the expansion wave, population growth rates approached $\lambda = 1$, indicating
511 population stasis driven by near-immortality and extremely rare recruitment.

512 *What is the seed dispersal kernel and how does it vary with maternal*
513 *plant size?*

514 WALD dispersal kernels were modeled using the properties of seeds and wind and
515 accounted for observed variation in wind speed, seed terminal velocity, and within-plant
516 seed release height. The resulting kernels were predicted to be strongly size dependent,
517 with taller plants having a greater probability of dispersing seeds longer distances (Fig.
518 5). However, predicted seed dispersal was highly local, with most seeds expected to
519 fall within one meter of parent plants for most sizes. Even for the very tallest shrub
520 we observed (1.96 m), only 6.2% of its seeds were predicted to fall more than 3 m away
521 and less than 1% were predicted to fall more than 6 m away (Fig. 5). Taller shrubs
522 also exhibited wider variance in their dispersal kernel, reflecting their wider range of
523 within-shrub seed release heights.

524 *What is the predicted rate of expansion and which lower-level processes*
525 *most strongly affect the expansion speed?*

526 The asymptotic speed of creosotebush encroachment, given the above demography and
527 dispersal patterns, was very slow. The mean asymptotic speed was 0.08 m/year and
528 the 5th–95th percentiles of the uncertainty distribution was 0.06–0.12 m/year (Fig. 6A).
529 The sensitivities of wavespeed spanned orders of magnitude, indicating strong inequal-
530 ity in the relative importance of the demography and dispersal processes controlling
531 expansion (Fig. 6B). Expansion speed was by far the most sensitive to the probability
532 of seedling recruitment (Fig. 6B), indicating that this life cycle transition imposes the
533 strongest constraint on encroachment. Sensitivity to survival ranked second, and since
534 nearly all mortality occurred at the smallest sizes this too can be interpreted as an early
535 life cycle constraint on expansion. The mean of growth ranked third and this was also
536 likely related to early plant survival, since increases in size allow small plants to reach
537 “protected” sizes given the strong size-dependence in survival.

538 **Discussion**

539 The encroachment of grasslands by woody plants is a worldwide phenomenon with
540 broad implications for biodiversity and ecosystem function. A theoretical perspective
541 rooted in spatial population biology brings attention to the combined influence of dis-
542 persal and density-dependent demography as critical controls on the occurrence and
543 pace of encroachment. Through this lens, we hypothesized that recent stasis at the grass-
544 shrub ecotone (Fig. 2) is driven by positive feedbacks that cause declines in fitness at
545 the low-density front. Instead, observational and experimental evidence indicate that
546 fitness was maximized in low-density plant neighborhoods. The creosotebush encroach-

ment wave is therefore predicted to be pulled by maximum demographic performance at the leading edge. However, our field-parameterized spatial integral projection model revealed that this wave is pulled at the very slow rate of 6–12 centimeters per year – so slow that this grass-shrub ecotone is predicted to be effectively stationary, consistent with observations. In fact, to our knowledge, this is the slowest plant population wavespeed estimated using SIPMs or their matrix model progenitors (Neubert and Caswell, 2000). Below, we discuss and interpret these key findings and their broader implications in greater detail.

Observational and experimental evidence strongly indicated that effects of shrub density were strongly negative in all vital rates and at all sizes. This was surprising given widespread evidence for positive feedbacks (which should generate low-density fitness penalties; i.e., Allee effects) in woody plant encroachment generally (D’odorico et al., 2013) and specifically in our creosotebush system (D’Odorico et al., 2010). How can we square these apparently conflicting results? First, it may be important to consider the distinction between “demographic” and “component” Allee effects (Stephens et al., 1999), which refer to effects that manifest in total fitness and components of fitness, respectively. That is, positive effects of conspecific density may occur, but in our measures of demographic performance these are swamped by stronger, counter-acting negative effects. It is worth noting that our demographic measurements are temporally coarse, reflecting aggregate performance over a full transition year. More mechanistic studies on finer time scales might reveal component Allee effects that are masked by strong net-negative density dependence. Second, many of the potential mechanisms for positive feedbacks at shrub-grass ecotones would manifest infrequently. For example, effects of shrub encroachment on microclimate (D’odorico et al., 2013) may promote shrub survival only in the face of rare climate events such as extreme low temperatures. Similarly,

572 positive feedbacks that occur via fire suppression (Collins et al., 2021; Ratajczak et al.,
573 2011) would only manifest on timescales that are inclusive of fire return intervals. These
574 considerations suggest that we may be more likely to detect positive density dependence
575 over longer time scales encompassing conditions that trigger positive feedbacks. This
576 leads to the hypothesis that the shrub encroachment wave is *usually* pulled but occasion-
577 ally pushed. To our knowledge such switches have never been empirically documented
578 in any expanding population but may be an important feature of expansion in fluctuating
579 environments.

580 The very low transplant survival and recruitment rates that we measured also call at-
581 tention to time scale. Previous studies suggest that creosotebush recruitment is strongly
582 episodic, likely in response to large, infrequent monsoon precipitation events (Allen et al.,
583 2008; Boyd and Brum, 1983; Moreno-de las Heras et al., 2016). Similar patterns of episodic
584 recruitment driven by large precipitation events have been observed in other cases of
585 woody plant encroachment in aridlands (Harrington, 1991; Weber-Grullon et al., 2022),
586 and relatively high transplant survival on the one transect that we planted immediately
587 following a large monsoon event anecdotally supports an important role for pulses of
588 soil moisture. With only four transition-years of demographic data, we chose to combine
589 information across years and build a deterministic model that averages over inter-annual
590 variability. However, the connection between shrub recruitment and monsoon precipita-
591 tion, combined with the observed and projected increase in the variability of monsoon
592 precipitation in our study region (Petrie et al., 2014; Rudgers et al., 2018), suggest that ex-
593 tending our deterministic model to accommodate inter-annual variability in climate and
594 climate-dependent vital rates will be a critical next step. Because our wavespeed esti-
595 mate is acutely sensitive to the seed-to-seedling transition, much more so than any other
596 demographic or dispersal process, we expect that a stochastic model incorporating many

years of data may yield a faster predicted expansion speed driven by rare pulses of recruitment (Ellner and Schreiber, 2012). Such pulses have clearly not occurred during our study years (2013–2017) or the preceding decade of transect re-surveys (2001–2012) and therefore we think the deterministic model is an adequate representation of recent conditions. However, our findings of pulled-wave dynamics and strong wavespeed sensitivity to seedling recruitment indicate that the present shrub ecotone is primed for expansion once the necessary climate conditions align, as they likely will in a more variable climate regime. While monsoon precipitation is a leading candidate for factors promoting seedling establishment, it is worth noting that our study years included both the lowest and second-highest amounts of monsoon precipitation in a 20-year record, and yet these events did not correlate with seedling recruitment on our transects (Appendix S2: Fig. S1). The conditions favoring recruitment and recruit survival may therefore be more complicated than the single driver of monsoon precipitation.

While not as strong a constraint based on our sensitivity analysis, limited dispersal ability also contributed to the very slow predicted speed of encroachment. Our findings of very limited dispersal are consistent with a previous study that found creosotebush seeds in the seed bank were found only beneath mature shrubs and not in nearby grass patches or inter-plant spaces (Moreno-de las Heras et al., 2016). Our mechanistic dispersal modeling assumes that wind is the sole dispersal vector. Previous work suggests that this modeling approach can accurately predict dispersal patterns for wind-dispersed plants (Skarpaas and Shea, 2007), yet in our system it may be important to consider secondary dispersal vectors. Boyd and Brum’s 1983 study of creosotebush reproductive biology described “contradiction in the literature about mode of dispersal”, citing evidence for a dominant role of wind but the additional possibility of seed movement by granivorous animals. Combining wind and animal dispersal vectors into a “total” dis-

persal kernel (Rogers et al., 2019) will be a valuable next step. Second, overland flow of runoff may contribute to secondary seed movement following initial deposition by wind (Thompson et al., 2014). Interestingly, seed movement from overland flow would be most likely following large monsoon events. Therefore, the same conditions that promote seedling recruitment may also promote long-distance dispersal, potentially amplifying a pulse of shrub encroachment (Ellner and Schreiber, 2012). Seeds may also be blown along the ground following initial deposition, which our model does not account for. The classic WALD dispersal model employed here assumes uniform grass cover, with seeds trapped below the height of this grass canopy. As in aridlands worldwide, our northern Chihuahuan Desert study region is characterized by a high percentage of bare ground, especially in areas of high creosotebush density (Fig. 1). New approaches are needed to extend mechanistic dispersal modeling to accommodate this feature of aridlands, as others have recognized (Thompson et al., 2014). The potential roles for both biotic and abiotic secondary dispersal vectors makes our dispersal kernel a conservative estimate of seed movement and highlights a need for further study of shrub seed dispersal.

Our model focused on intra-specific density dependence but inter-specific plant-plant interactions may be an important element of shrub encroachment, or lack thereof. For example, over-grazing is a hypothesized driver of shrub encroachment due to release from grass competition and reduction of grassland fires (Van Auken, 2000). Our shrub encroachment model considered only one “side” of the grass-shrub ecotone, assuming that the shrub population spreads into empty space. Explicit consideration of grass competition or facilitation may enrich our understanding of shrub advance or stasis in this and other systems (Sankaran et al., 2004). However, our transplant experiment suggested weak negative effects of grass cover on seedling survival (Appendix S3: Fig.

647 S1B). Similarly, grass competition had no effect on germination and survival of mesquite
648 (*Prosopis glandulosa*) shrubs in Chihuahuan Desert grassland (Weber-Grullon et al., 2022).
649 While our current data do not allow us to quantify whether and how strongly resident
650 grasses may slow down shrub encroachment, we can infer that competitive effects of
651 grasses on shrubs are weaker than competitive effects of shrubs on shrubs. Therefore
652 our conclusion that the encroachment wave is pulled implicitly accounts for any effects
653 of grass cover.

654 While our data reveal strong negative density dependence, we know little about the
655 underlying mechanisms that give rise to this pattern. What is it about high shrub density
656 environments that suppress survival and reproduction? The abundance of bare ground
657 in core shrubland suggests that shrubs do not compete for space. However, Brisson
658 and Reynolds (1994) found strong competition for space belowground, with crowded
659 neighborhoods constraining creosotebush root systems. Also, root development of cre-
660 osotebush seedlings can respond rapidly to the availability of soil moisture (Obrist and
661 Arnone III, 2003), suggesting that competition for water may be another element of den-
662 sity dependence. Finally, negative density dependence in plants may also be mediated by
663 consumers or soil microbes. Better understanding the environmental drivers of density
664 dependence will enable better prediction for how the encroachment wave may respond
665 to future environmental change.

666 Our model was parameterized specifically for the creosotebush system, but the body
667 of theory upon which it is based is broadly applicable to other woody encroachment
668 systems. Examples from the literature provide interesting points of similarity and con-
669 trast. Encroaching *Acacia mellifera* in Namibian savanna experience negative density de-
670 pendence in seedling survival (Joubert et al., 2013), and leading-edge colonists at boreal
671 treelines experience a growth advantage over established trees (Dial et al., 2022); both are

672 consistent with pulled-wave encroachment dynamics, as we observed in creosotebush.
673 On the other hand, *Acacia drepanolobium* in East African savanna experiences positive
674 feedbacks that arise from mutualism with defensive ants (higher-density tree aggrega-
675 tions support larger populations of defenders), which promotes the stability of mon-
676 odominant stands but generate pushed-wave dynamics that limit encroachment (Ken-
677 fack et al., 2021). In another pushed-wave example, woody plants in Brazilian Cerrado
678 facilitate both the arrival and establishment of other woody species by attracting seed-
679 dispersing birds and ameliorating stressful soil conditions (Abreu et al., 2021). Clearly,
680 the pace and underlying mechanisms of encroachment may exhibit wide variation across
681 species or systems depending on the nature of density-dependent feedbacks as well as
682 external drivers such as fire suppression, grazing, and climate change. The general
683 demography-dispersal framework developed here may provide a unifying lens to un-
684 derstand and predict woody encroachment in diverse systems, from arctic treeline to
685 aridland savanna to salt marsh ecosystems (Kelleway et al., 2017). Furthermore, trait-
686 based approaches may help explain variation in encroachment speed across species or
687 systems and identify which are prone to pushed or pulled dynamics. For example, in two
688 of the examples above, reliance on animal mutualists for defense or dispersal generated
689 positive density-dependent feedbacks.

690 *Conclusions.* Understanding and predicting the dynamics of woody-herbaceous eco-
691 tones requires that we build knowledge of the fates of the rare individuals that disperse
692 from core habitat and cross habitat boundaries. For a creosotebush, there is no better
693 place to be than alone in a grassland, and that key result governs the spatial dynamics
694 of this population. We found that the wave of creosotebush expansion into Chihuahuan
695 desert grassland is pulled by peak fitness at the leading edge. However, it is pulled so
696 slowly that it is effectively stalled, a model-derived prediction that recapitulates obser-

697 vations on the ground. Had we only relied on the re-survey data without insight from
698 the mechanistic model we might have concluded that the creosotebush ecotone is stable
699 at its current boundary. Instead, acute sensitivity of a slow wave to seedling recruitment
700 leaves this system poised for pulses of expansion under the right conditions; what ex-
701 actly those conditions are is not yet fully resolved. We suggest that the concepts and
702 tools of spatial population biology may facilitate advances in the study and management
703 of woody plant encroachment, which, like all spreading populations, must be driven by
704 birth, death, and movement.

705 **Acknowledgements**

706 This research was supported by the Sevilleta LTER program (NSF DEB awards 1655499,
707 1748133) and by NSF DEB award 1856383. We are grateful to Andrew Bibian, Aldo Com-
708 pagnoni, Kevin Czachura, Marion Donald, Kory Kolis, Johanna Ohm, Rande Patterson,
709 Eréndira Quintana Morales, Olivia Ragni, Emily Schultz, and Charlene Thomas for their
710 contributions to field data collection. Kat Shea and Olav Skarpaas provided helpful guid-
711 ance on dispersal modeling. Two anonymous reviewers provided valuable feedback on
712 the manuscript. This research was permitted by the US Fish and Wildlife Service with a
713 Special Use Permit.

714 **Author contributions**

715 All authors contributed to study design. THD and TEXM led data analysis, modeling,
716 and writing early drafts of the manuscript. All authors participated in preparing the
717 manuscript for submission.

Literature Cited

- Abreu, R. C., G. Durigan, A. C. Melo, N. A. Pilon, and W. A. Hoffmann. 2021. Facilitation by isolated trees triggers woody encroachment and a biome shift at the savanna–forest transition. *Journal of Applied Ecology* **58**:2650–2660.
- Allen, A., W. Pockman, C. Restrepo, and B. Milne. 2008. Allometry, growth and population regulation of the desert shrub *Larrea tridentata*. *Functional Ecology* pages 197–204.
- Bowers, J. E., R. M. Turner, and T. L. Burgess. 2004. Temporal and spatial patterns in emergence and early survival of perennial plants in the Sonoran Desert. *Plant Ecology* **172**:107–119.
- Boyd, R. S., and G. D. Brum. 1983. Postdispersal reproductive biology of a Mojave Desert population of *Larrea tridentata* (Zygophyllaceae). *American Midland Naturalist* pages 25–36.
- Brandt, J. S., M. A. Haynes, T. Kuemmerle, D. M. Waller, and V. C. Radeloff. 2013. Regime shift on the roof of the world: Alpine meadows converting to shrublands in the southern Himalayas. *Biological Conservation* **158**:116–127.
- Brisson, J., and J. F. Reynolds. 1994. The effect of neighbors on root distribution in a creosotebush (*Larrea tridentata*) population. *Ecology* **75**:1693–1702.
- Buffington, L. C., and C. H. Herbel. 1965. Vegetational changes on a semidesert grassland range from 1858 to 1963. *Ecological monographs* **35**:139–164.
- Cabral, A., J. De Miguel, A. Rescia, M. Schmitz, and F. Pineda. 2003. Shrub encroachment in Argentinean savannas. *Journal of Vegetation Science* **14**:145–152.

740 Collins, S. L., J. B. Nippert, J. M. Blair, J. M. Briggs, P. Blackmore, and Z. Ratajczak.
 741 2021. Fire frequency, state change and hysteresis in tallgrass prairie. *Ecology Letters*
 742 **24**:636–647.

743 Dial, R. J., C. T. Maher, R. E. Hewitt, and P. F. Sullivan. 2022. Sufficient conditions for
 744 rapid range expansion of a boreal conifer. *Nature* **608**:546–551.

745 D’Odorico, P., J. D. Fuentes, W. T. Pockman, S. L. Collins, Y. He, J. S. Medeiros,
 746 S. DeWekker, and M. E. Litvak. 2010. Positive feedback between microclimate and
 747 shrub encroachment in the northern Chihuahuan desert. *Ecosphere* **1**:1–11.

748 D’odorico, P., Y. He, S. Collins, S. F. De Wekker, V. Engel, and J. D. Fuentes. 2013.
 749 Vegetation–microclimate feedbacks in woodland–grassland ecotones. *Global Ecology*
 750 *and Biogeography* **22**:364–379.

751 D’Odorico, P., G. S. Okin, and B. T. Bestelmeyer. 2012. A synthetic review of feedbacks
 752 and drivers of shrub encroachment in arid grasslands. *Ecohydrology* **5**:520–530.

753 Drees, T. H., and T. E. Miller, 2023. Code from: Demography and dispersal at a grass-
 754 shrub ecotone: a spatial integral projection model for woody plant encroachment.
 755 <https://doi.org/10.5281/zenodo.7739604>.

756 Duran, K. L., T. K. Lowrey, R. R. Parmenter, and P. O. Lewis. 2005. Genetic diversity in
 757 Chihuahuan Desert populations of creosotebush (Zygophyllaceae: *Larrea tridentata*).
 758 *American Journal of Botany* **92**:722–729.

759 Ellner, S. P., D. Z. Childs, M. Rees, et al. 2016. Data-driven modelling of structured
 760 populations. *A practical guide to the Integral Projection Model*. Cham: Springer .

761 Ellner, S. P., and S. J. Schreiber. 2012. Temporally variable dispersal and demography can
 762 accelerate the spread of invading species. *Theoretical Population Biology* **82**:283–298.

- 763 Gandhi, S. R., E. A. Yurtsev, K. S. Korolev, and J. Gore. 2016. Range expansions transition
764 from pulled to pushed waves as growth becomes more cooperative in an experimental
765 microbial population. *Proceedings of the National Academy of Sciences* **113**:6922–6927.
- 766 Gardner, J. L. 1951. Vegetation of the creosotebush area of the Rio Grande Valley in New
767 Mexico. *Ecological Monographs* **21**:379–403.
- 768 Gibbens, R., R. McNeely, K. Havstad, R. Beck, and B. Nolen. 2005. Vegetation changes in
769 the Jornada Basin from 1858 to 1998. *Journal of Arid Environments* **61**:651–668.
- 770 Goslee, S., K. Havstad, D. Peters, A. Rango, and W. Schlesinger. 2003. High-resolution
771 images reveal rate and pattern of shrub encroachment over six decades in New Mexico,
772 USA. *Journal of Arid Environments* **54**:755–767.
- 773 Grover, H. D., and H. B. Musick. 1990. Shrubland encroachment in southern New Mex-
774 ico, USA: an analysis of desertification processes in the American Southwest. *Climatic*
775 *change* **17**:305–330.
- 776 Harrington, G. N. 1991. Effects of soil moisture on shrub seedling survival in semi-arid
777 grassland. *Ecology* **72**:1138–1149.
- 778 Huang, H., L. D. Anderegg, T. E. Dawson, S. Mote, and P. D’Odorico. 2020. Critical tran-
779 sition to woody plant dominance through microclimate feedbacks in North American
780 coastal ecosystems. *Ecology* **101**:e03107.
- 781 Jongejans, E., K. Shea, O. Skarpaas, D. Kelly, and S. P. Ellner. 2011. Importance of
782 individual and environmental variation for invasive species spread: a spatial integral
783 projection model. *Ecology* **92**:86–97.
- 784 Joubert, D. F., G. Smit, and M. T. Hoffman. 2013. The influence of rainfall, competition

785 and predation on seed production, germination and establishment of an encroaching
786 Acacia in an arid Namibian savanna. *Journal of Arid Environments* **91**:7–13.

787 Katul, G., A. Porporato, R. Nathan, M. Siqueira, M. Soons, D. Poggi, H. Horn, and S. A.
788 Levin. 2005. Mechanistic analytical models for long-distance seed dispersal by wind.
789 *The American Naturalist* **166**:368–381.

790 Keitt, T. H., M. A. Lewis, and R. D. Holt. 2001. Allee effects, invasion pinning, and
791 species' borders. *The American Naturalist* **157**:203–216.

792 Kelleway, J. J., K. Cavanaugh, K. Rogers, I. C. Feller, E. Ens, C. Doughty, and N. Saintilan.
793 2017. Review of the ecosystem service implications of mangrove encroachment into
794 salt marshes. *Global Change Biology* **23**:3967–3983.

795 Kenfack, D., G. Arellano, S. Kibet, D. Kimuyu, and P. Musili. 2021. Understanding the
796 monodominance of *Acacia drepanolobium* in East African savannas: insights from
797 demographic data. *Trees* **35**:1439–1450.

798 Knapp, A. K., J. M. Briggs, S. L. Collins, S. R. Archer, M. S. BRET-HARTE, B. E. Ewers,
799 D. P. Peters, D. R. Young, G. R. Shaver, E. Pendall, et al. 2008. Shrub encroachment in
800 North American grasslands: shifts in growth form dominance rapidly alters control of
801 ecosystem carbon inputs. *Global Change Biology* **14**:615–623.

802 Kot, M., M. A. Lewis, and P. van den Driessche. 1996. Dispersal data and the spread of
803 invading organisms. *Ecology* **77**:2027–2042.

804 Lewis, M., and P. Kareiva. 1993. Allee dynamics and the spread of invading organisms.
805 *Theoretical Population Biology* **43**:141–158.

806 Lewis, M. A., M. G. Neubert, H. Caswell, J. S. Clark, and K. Shea, 2006. A guide to cal-

807 culating discrete-time invasion rates from data. Pages 169–192 *in* Conceptual ecology
808 and invasion biology: reciprocal approaches to nature. Springer.

809 Mabry, T. J., J. H. Hunziker, D. Difeo Jr, et al. 1978. Creosote bush: biology and chemistry
810 of *Larrea* in New World deserts. Dowden, Hutchinson & Ross, Inc.

811 Maddox, J. C., and S. Carlquist. 1985. Wind dispersal in Californian desert plants:
812 experimental studies and conceptual considerations. *Aliso: A Journal of Systematic*
813 and Evolutionary Botany **11**:77–96.

814 McAuliffe, J., E. Hamerlynck, and M. Eppes. 2007. Landscape dynamics fostering the
815 development and persistence of long-lived creosotebush (*Larrea tridentata*) clones in
816 the Mojave Desert. *Journal of Arid Environments* **69**:96–126.

817 Moore, D., and K. Hall, 2022. Meteorology Data from the Sevilleta Na-
818 tional Wildlife Refuge, New Mexico. Environmental Data Initiative.
819 <https://doi.org/10.6073/pasta/d56307b398e28137dabaa6994f0f5f92>.

820 Moreno-de las Heras, M., L. Turnbull, and J. Wainwright. 2016. Seed-bank structure
821 and plant-recruitment conditions regulate the dynamics of a grassland-shrubland Chi-
822 huahuan ecotone. *Ecology* **97**:2303–2318.

823 Morford, S. L., B. W. Allred, D. Twidwell, M. O. Jones, J. D. Maestas, C. P. Roberts, and
824 D. E. Naugle. 2022. Herbaceous production lost to tree encroachment in United States
825 rangelands. *Journal of Applied Ecology* **59**:2971–2982.

826 Nathan, R., G. G. Katul, G. Bohrer, A. Kuparinen, M. B. Soons, S. E. Thompson, A. Trakht-
827 enbrot, and H. S. Horn. 2011. Mechanistic models of seed dispersal by wind. *Theoret-*
828 ical Ecology **4**:113–132.

- Neubert, M. G., and H. Caswell. 2000. Demography and dispersal: calculation and sensitivity analysis of invasion speed for structured populations. *Ecology* **81**:1613–1628.
- Obrist, D., and J. Arnone III. 2003. Increasing CO₂ accelerates root growth and enhances water acquisition during early stages of development in *Larrea tridentata*. *New Phytologist* **159**:175–184.
- Ochocki, B. M., T. H. Drees, and T. E. Miller, 2023. Density-dependent demography of creosote bush (*Larrea tridentata*) along grass-shrub ecotones. <https://doi.org/10.6073/pasta/ca53c16f16dcf9fb11f3ee99ea5445ac>.
- Pan, S., and G. Lin. 2012. Invasion traveling wave solutions of a competitive system with dispersal. *Boundary Value Problems* **2012**:120.
- Parizek, B., C. M. Rostagno, and R. Sottini. 2002. Soil erosion as affected by shrub encroachment in northeastern Patagonia. *Rangeland Ecology & Management/Journal of Range Management Archives* **55**:43–48.
- Peters, D. P., and J. Yao. 2012. Long-term experimental loss of foundation species: consequences for dynamics at ecotones across heterogeneous landscapes. *Ecosphere* **3**:1–23.
- Petrie, M., S. Collins, D. Gutzler, and D. Moore. 2014. Regional trends and local variability in monsoon precipitation in the northern Chihuahuan Desert, USA. *Journal of Arid Environments* **103**:63–70.
- Ratajczak, Z., J. B. Nippert, and S. L. Collins. 2012. Woody encroachment decreases diversity across North American grasslands and savannas. *Ecology* **93**:697–703.

- 851 Ratajczak, Z., J. B. Nippert, J. C. Hartman, and T. W. Ocheltree. 2011. Positive feedbacks
852 amplify rates of woody encroachment in mesic tallgrass prairie. *Ecosphere* **2**:1–14.
- 853 Ravi, S., P. D’Odorico, S. L. Collins, and T. E. Huxman. 2009. Can biological invasions
854 induce desertification? *The New Phytologist* **181**:512–515.
- 855 Reed, M., L. Stringer, A. Dougill, J. Perkins, J. Atlhopheng, K. Mulale, and N. Favretto.
856 2015. Reorienting land degradation towards sustainable land management: Linking
857 sustainable livelihoods with ecosystem services in rangeland systems. *Journal of envi-
858 ronmental management* **151**:472–485.
- 859 Reynolds, J. F., R. A. Virginia, P. R. Kemp, A. G. De Soyza, and D. C. Tremmel. 1999.
860 Impact of drought on desert shrubs: effects of seasonality and degree of resource
861 island development. *Ecological Monographs* **69**:69–106.
- 862 Rogers, H. S., N. G. Beckman, F. Hartig, J. S. Johnson, G. Pufal, K. Shea, D. Zurell, J. M.
863 Bullock, R. S. Cantrell, B. Loiselle, et al. 2019. The total dispersal kernel: a review and
864 future directions. *AoB Plants* **11**:plz042.
- 865 Roques, K., T. O’connor, and A. R. Watkinson. 2001. Dynamics of shrub encroachment in
866 an African savanna: relative influences of fire, herbivory, rainfall and density depen-
867 dence. *Journal of Applied Ecology* **38**:268–280.
- 868 Rudgers, J. A., Y. A. Chung, G. E. Maurer, D. I. Moore, E. H. Muldavin, M. E. Litvak,
869 and S. L. Collins. 2018. Climate sensitivity functions and net primary production: a
870 framework for incorporating climate mean and variability. *Ecology* **99**:576–582.
- 871 Sankaran, M., J. Ratnam, and N. P. Hanan. 2004. Tree–grass coexistence in savannas
872 revisited—insights from an examination of assumptions and mechanisms invoked in
873 existing models. *Ecology letters* **7**:480–490.

- 874 Schlesinger, W. H., and A. M. Pilmanis. 1998. Plant-soil interactions in deserts. *Biogeo-*
875 *chemistry* **42**:169–187.
- 876 Schlesinger, W. H., J. A. Raikes, A. E. Hartley, and A. F. Cross. 1996. On the spatial
877 pattern of soil nutrients in desert ecosystems: ecological archives E077-002. *Ecology*
878 **77**:364–374.
- 879 Schlesinger, W. H., J. F. Reynolds, G. L. Cunningham, L. F. Huenneke, W. M. Jarrell, R. A.
880 Virginia, and W. G. Whitford. 1990. Biological feedbacks in global desertification.
881 *Science* **247**:1043–1048.
- 882 Sirami, C., and A. Monadjem. 2012. Changes in bird communities in Swaziland savannas
883 between 1998 and 2008 owing to shrub encroachment. *Diversity and Distributions*
884 **18**:390–400.
- 885 Skarpaas, O., and K. Shea. 2007. Dispersal patterns, dispersal mechanisms, and invasion
886 wave speeds for invasive thistles. *The American Naturalist* **170**:421–430.
- 887 Stephens, P. A., W. J. Sutherland, and R. P. Freckleton. 1999. What is the Allee effect?
888 *Oikos* pages 185–190.
- 889 Sullivan, L. L., B. Li, T. E. Miller, M. G. Neubert, and A. K. Shaw. 2017. Density depen-
890 dence in demography and dispersal generates fluctuating invasion speeds. *Proceed-*
891 *ings of the National Academy of Sciences* **114**:5053–5058.
- 892 Taylor, C. M., and A. Hastings. 2005. Allee effects in biological invasions. *Ecology Letters*
893 **8**:895–908.
- 894 Thompson, S. E., S. Assouline, L. Chen, A. Trahktenbrot, T. Svoray, and G. G. Katul. 2014.
895 Secondary dispersal driven by overland flow in drylands: Review and mechanistic
896 model development. *Movement ecology* **2**:7.

- 897 Trollope, W., F. Hobson, J. Danckwerts, and J. Van Niekerk. 1989. Encroachment and
898 control of undesirable plants. *Veld management in the Eastern Cape* pages 73–89.
- 899 Turnbull, L., J. Wainwright, and R. E. Brazier. 2010. Changes in hydrology and erosion
900 over a transition from grassland to shrubland. *Hydrological Processes: An Interna-*
901 *tional Journal* **24**:393–414.
- 902 Van Auken, O. 2009. Causes and consequences of woody plant encroachment into
903 western North American grasslands. *Journal of environmental management* **90**:2931–
904 2942.
- 905 Van Auken, O. W. 2000. Shrub invasions of North American semiarid grasslands. *Annual*
906 *review of ecology and systematics* **31**:197–215.
- 907 Vasek, F. C. 1980. Creosote bush: Long-lived clones in the Mojave Desert. *American*
908 *Journal of Botany* **67**:246–255.
- 909 Veit, R. R., and M. A. Lewis. 1996. Dispersal, population growth, and the Allee effect: dy-
910 namics of the house finch invasion of eastern North America. *The American Naturalist*
911 **148**:255–274.
- 912 Wang, M.-H., M. Kot, and M. G. Neubert. 2002. Integrodifference equations, Allee effects,
913 and invasions. *Journal of mathematical biology* **44**:150–168.
- 914 Weber-Grullon, L., L. Gherardi, W. A. Rutherford, S. R. Archer, and O. E. Sala. 2022.
915 Woody-plant encroachment: Precipitation, herbivory, and grass-competition interact
916 to affect shrub recruitment. *Ecological Applications* **32**:e2536.
- 917 Wilcox, B. P., A. Birt, S. D. Fuhlendorf, and S. R. Archer. 2018. Emerging frameworks for
918 understanding and mitigating woody plant encroachment in grassy biomes. *Current*
919 *Opinion in Environmental Sustainability* **32**:46–52.

- 920 Williams, J. L., T. E. Miller, and S. P. Ellner. 2012. Avoiding unintentional eviction from
921 integral projection models. *Ecology* **93**:2008–2014.
- 922 Wood, S. 2017. *Generalized Additive Models: An Introduction with R*. 2 edition. Chap-
923 man and Hall/CRC.

Figure legends

Figure 1. Example of an ecotone transect spanning gradients of creosotebush and black grama grass at Sevilleta National Wildlife Refuge, a Long-Term Ecological Research (LTER) site in central New Mexico, US. Photo credit: T.E.X. Miller.

Figure 2. Surveys of creosotebush percent cover along two permanent transects (A,B) in 2001 and 2013. In summer 2001, shrub percent cover was recorded along two permanent 1000-m transects that spanned the shrub-grass ecotone. Surveys were conducted again in summer 2013. At every 10 meters, shrub cover was recorded in nine cover classes (<1%, 1–4%, 5–10%, 10–25%, 25–33%, 33–50%, 50–75%, 75–95%, >95%). This figure shows mid-point values of these cover classes at each meter location for both transects and years.

Figure 3. Size- and density-dependence in demographic vital rates. **A** Probability of survival from natural population census and transplant experiment (black line), **B** Mean and variance (inset) of size conditional on previous size, **C** Probability of flowering, **D** Flower and fruit production, **E** Probability of recruitment per seed, **F** Recruit size. In **A–D**, colored lines indicate four size groups (red is largest, blue is smallest), discretized for data visualization only. In all panels, weighted density is the sum of all plant sizes $\log(\text{cm}^3)$ within the same 5-m window as the census individual. In panels **A** and **C**, points indicate binned means and point size is proportional to sample size for the mean.

Figure 4. Density dependence in the asymptotic population growth rate (λ). Gray lines show bootstrap replicates and the black lines shows predictions from full demographic data set. Weighted deighted density is the sum of all plant sizes $\log(\text{cm}^3)$ within 5-m windows.

Figure 5. Predicted WALD dispersal kernels for four shrub heights corresponding to the 25th, 50th, 75th, and 100th (maximum) percentiles of the observed size distribution. We

948 assume that heights below 15 cm have effectively no seed movement due to interference
949 with the grass layer.

950 **Figure 6.** A, Asymptotic speed of creosotebush encroachment. The distribution reflects
951 parameter and model uncertainties quantified via bootstrapping and stochastic sampling
952 from seed dispersal kernels. B, Sensitivities of wavespeed to demography and disper-
953 sal processes. For size-dependent functions (growth, survival, flowering, and fertility)
954 sensitivity was calculate by perturbing the entire function across all sizes.

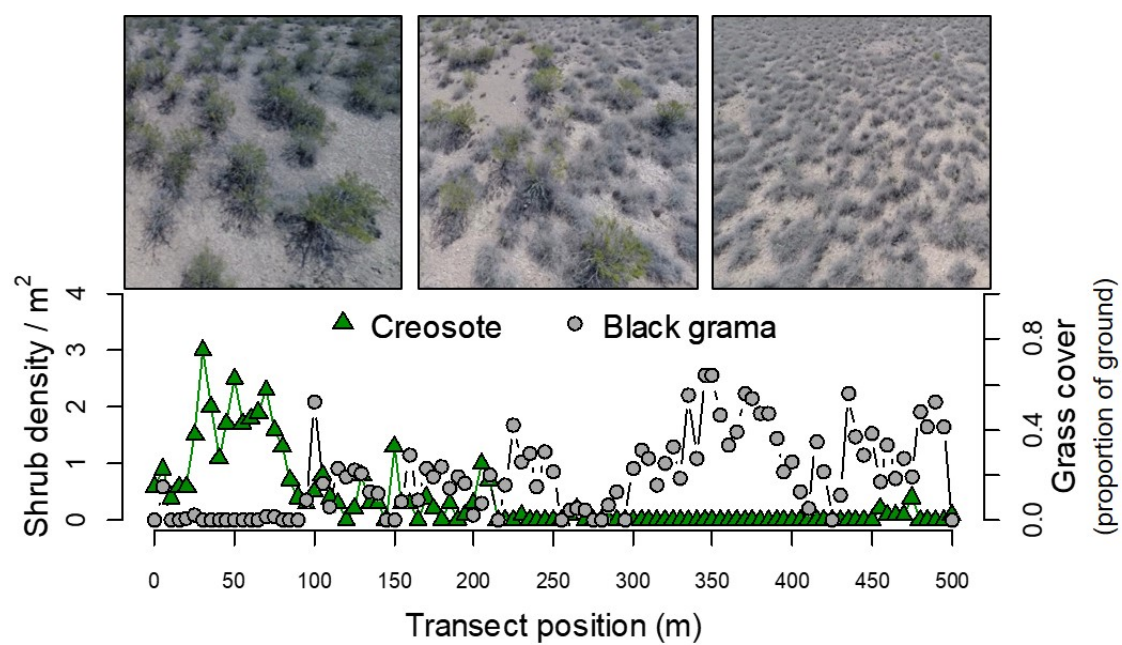


Figure 1

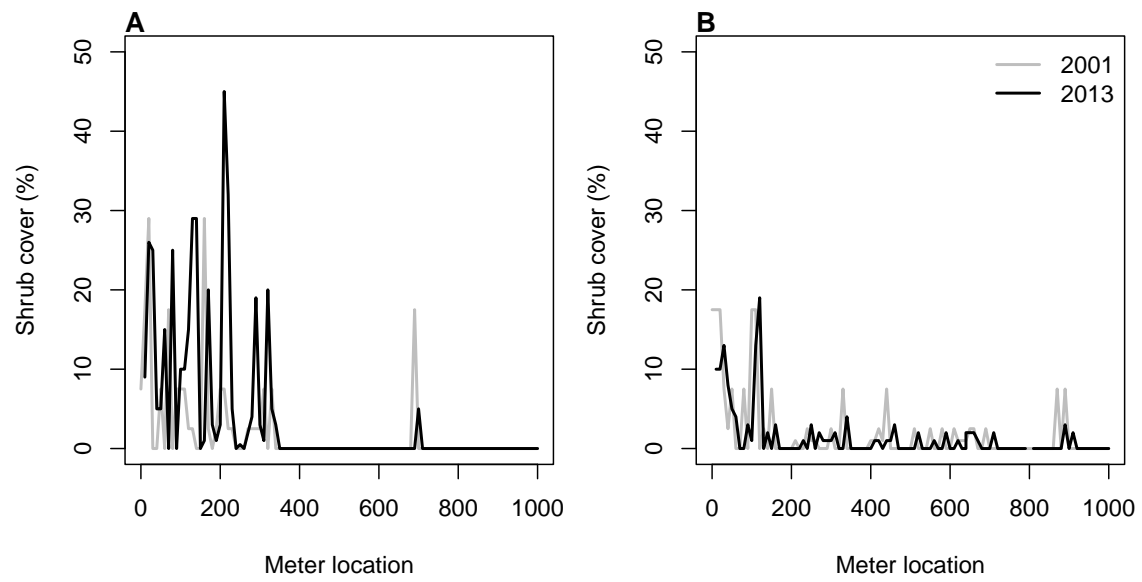


Figure 2

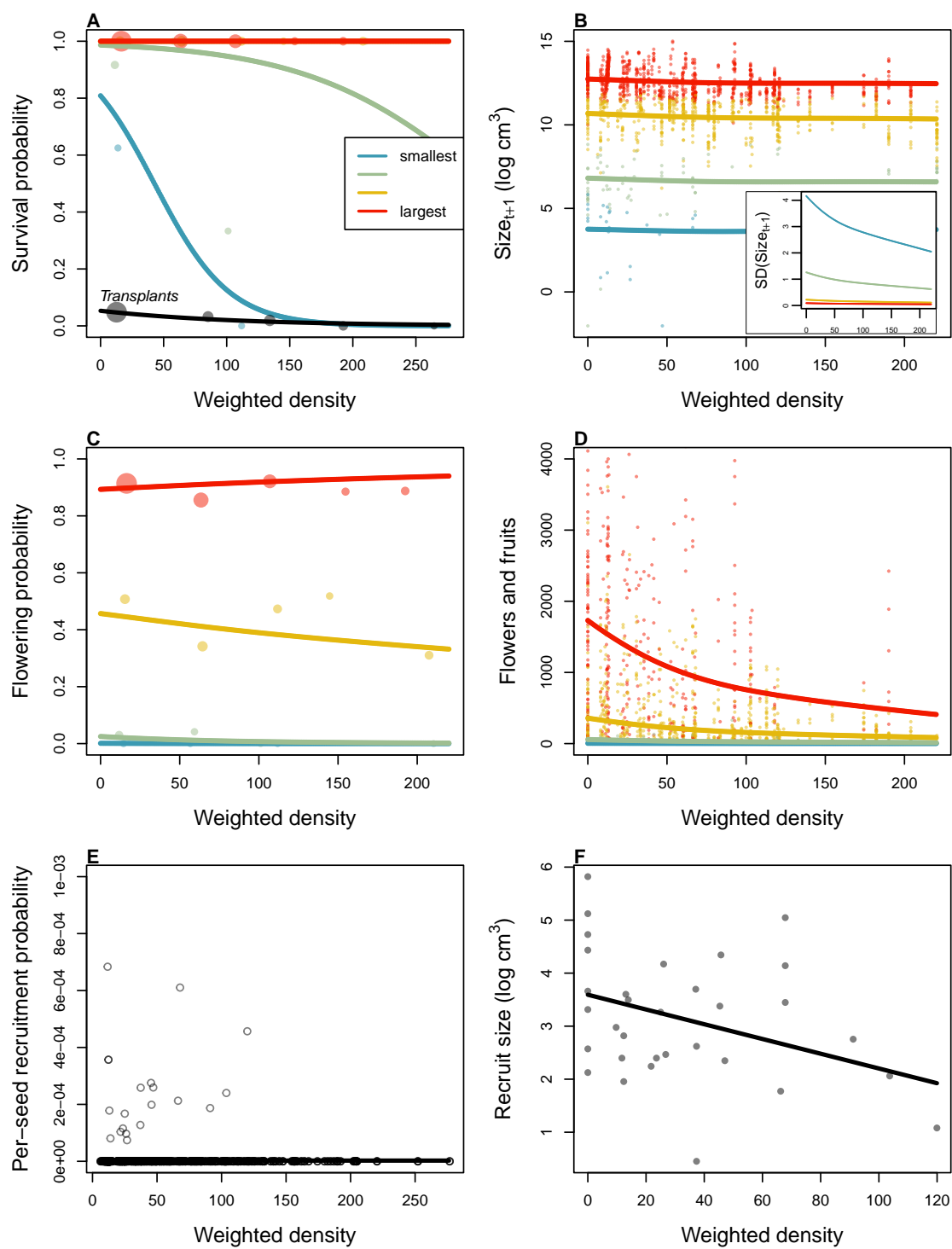


Figure 3

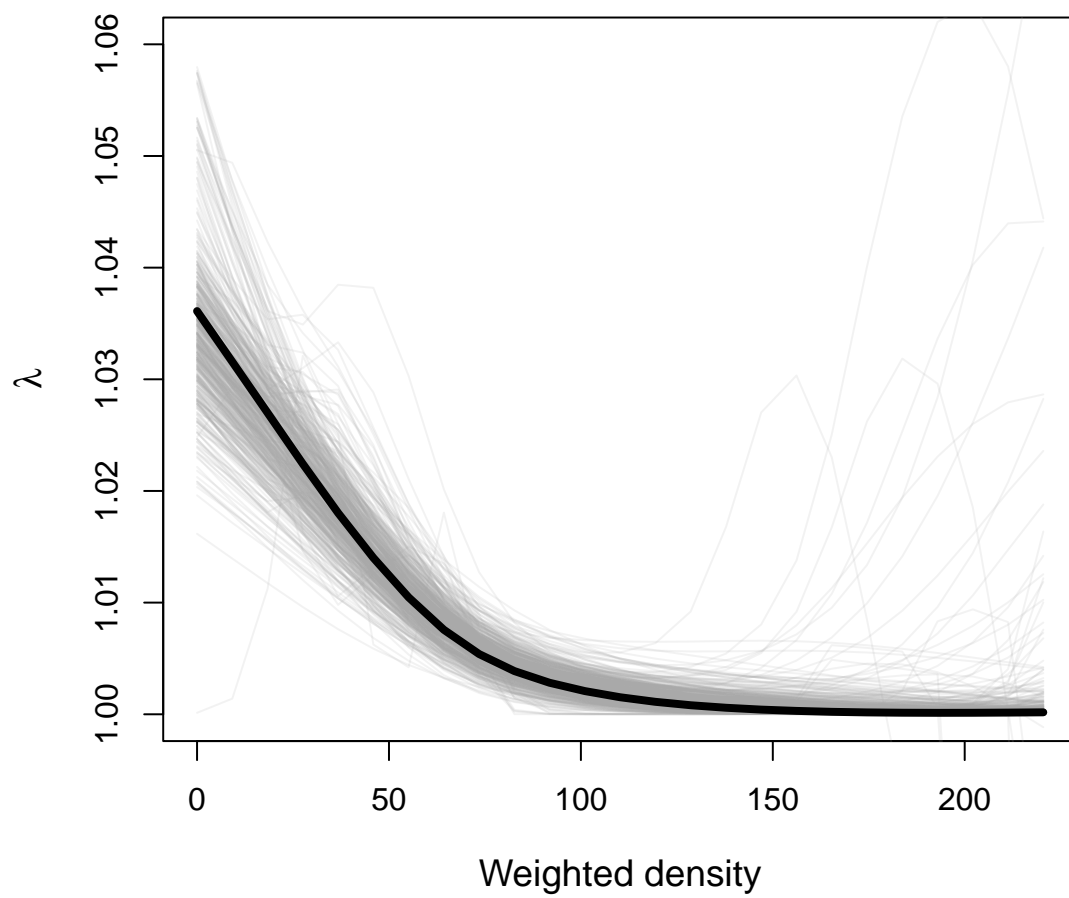


Figure 4

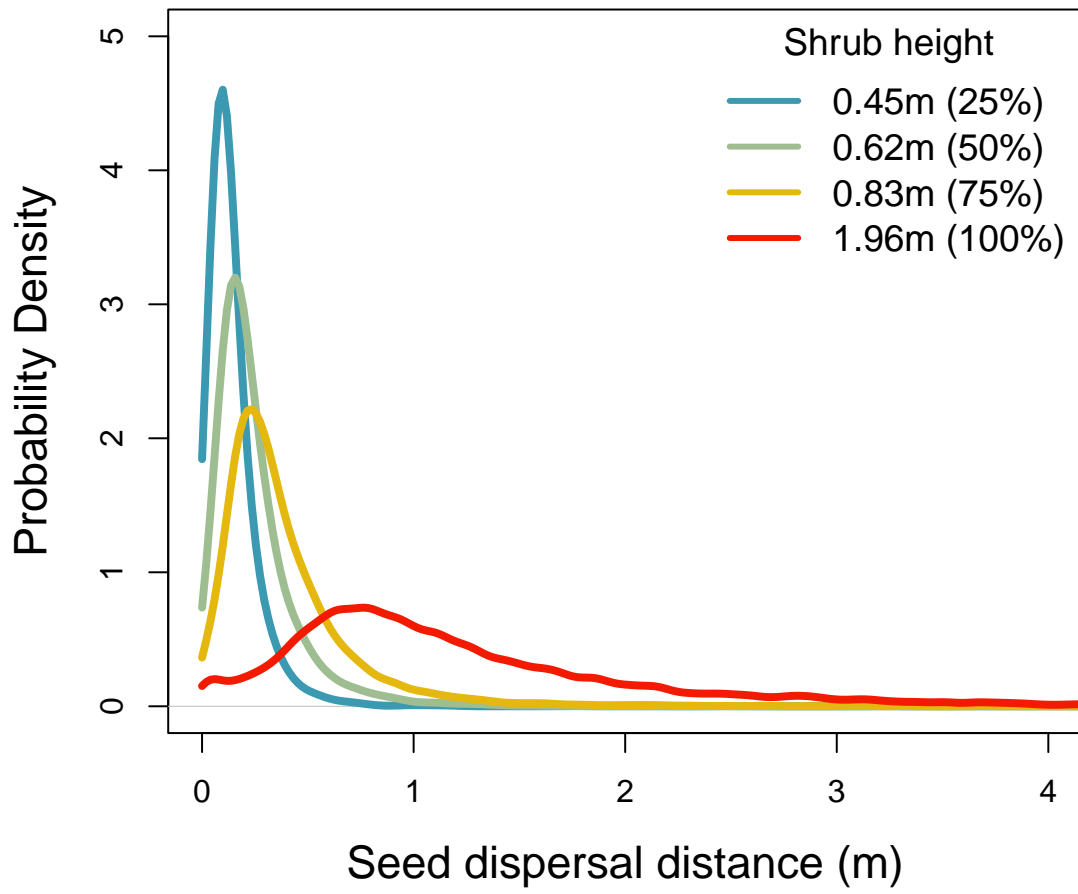


Figure 5

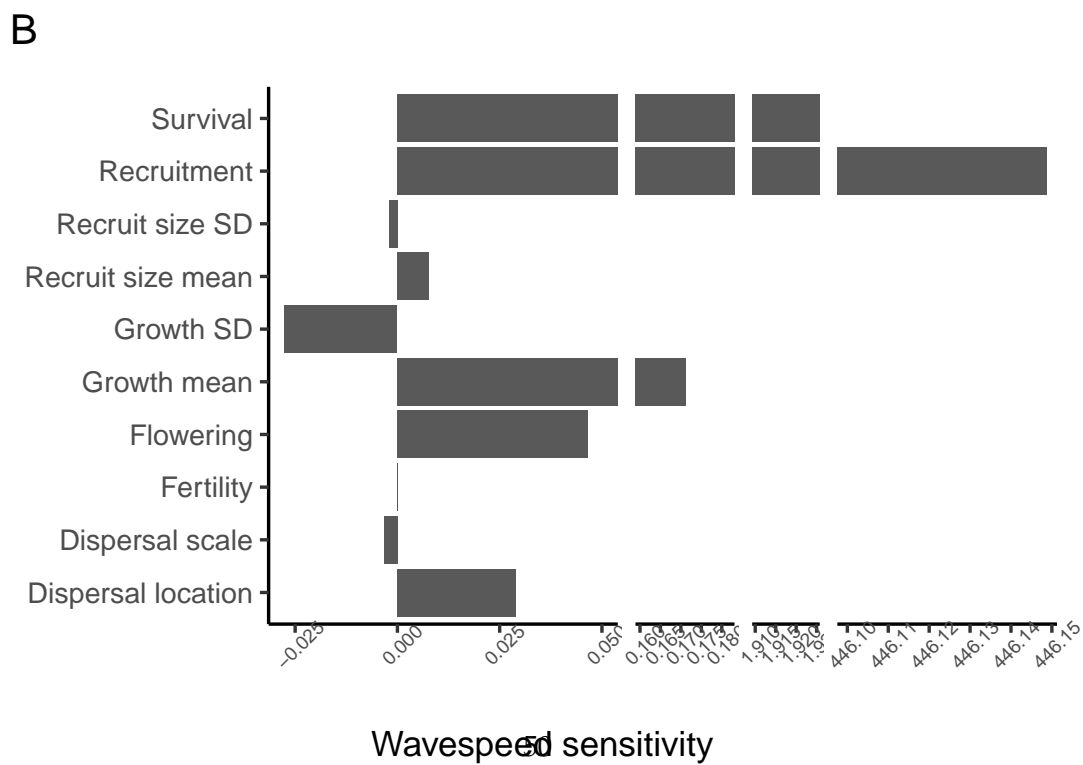
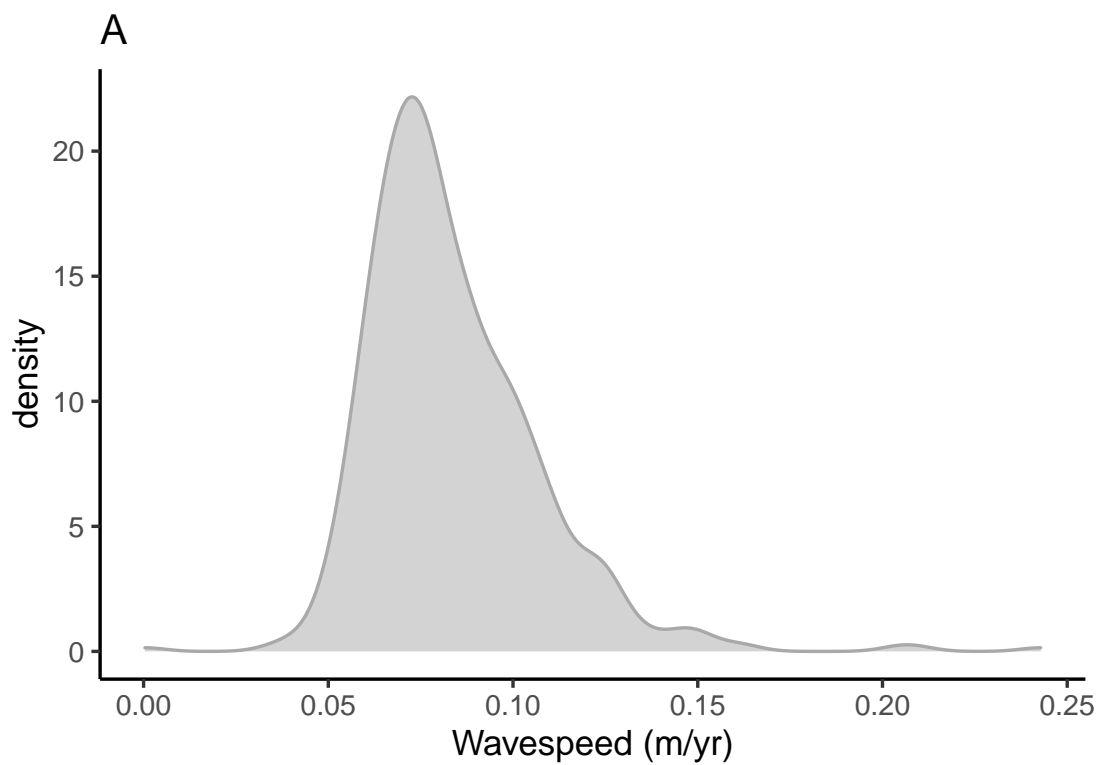


Figure 6